SUPPLEMENT TO THE *WELDING JOURNAL*, DECEMBER 2009
Sponsored by the American Welding Society and the Welding Research Council

A Novel Preweld Laser Surface Treatment for Enhanced Intergranular Corrosion Resistance of Austenitic Stainless Steel Weldments

A new scheme of preweld laser surface treatment is developed for Type 304 stainless steel for enhanced resistance against HAZ sensitization and intergranular corrosion

BY R. KAUL, N. PARVATHAVARTHINI, P. GANESH, S. V. MULKI, I. SAMAJDAR, R. K. DAYAL, AND L. M. KUKREJA

ABSTRACT

This paper describes the development of a new prewelding laser surface melting treatment scheme to suppress sensitization in the heat-affected zone of gas tungsten arc weldment of Type 304 stainless steel. The results of the present study, performed on 6-mm-thick medium-carbon (0.044 wt-%) and 10-mm-thick high-carbon (0.1 wt-%) Type 304 stainless steel sheets, established that surface modification engineered by CO_2 laser treatment is highly effective in suppressing heat-affected zone sensitization during subsequent gas tungsten arc welding. Laser surface treated heat-affected zone of gas tungsten arc weldment exhibited a significantly lower degree of sensitization and susceptibility to intergranular corrosion than those of untreated heat-affected zone. This is attributed to higher fraction of Σ1 subgrain boundaries introduced by laser-assisted melting and resolidification.

R. KAUL (rkaul@rrcat.gov.in), P. GANESH, and L. M. KUKREJA are with Laser Materials Processing Division, Raja Ramanna Centre for Advanced Technology, Indore, India. N. PARVATHAVARTHINI and R. K. DAYAL are with Corrosion Science and Technology Division, Indira Gandhi Centre for Atomic Research, Kalpakkam, India. S. V. MULKI and I. SAMAJDAR are with Department of Metallurgical Engineering and Materials Science, Indian Institute of Technology, Mumbai, India.

Introduction

Austenitic stainless steels (SS), in spite of having excellent ductility and general corrosion resistance, are particularly susceptible to localized corrosion, e.g., crevice, pitting, intergranular corrosion (IGC), and stress corrosion cracking (SCC). Susceptibility to localized corrosion and SCC is mainly caused by the presence of chloride ions in the associated environment. In nuclear fuel reprocessing, waste management industries, and in many chemical industries, the main corrosion problem is IGC when nitric acid is used as the process fluid. Sensitization is also the prime cause for intergranular stress corrosion cracking (IGSCC) of SS weldments in certain environments, e.g., oxidizing water in boiling water reactors (Ref. 1). Intergranular corrosion of austenitic SS arises from intergranular precipitation of chromium-rich carbides in the temperature range of 773–1073 K. Intergranular carbide precipitation is accompanied by the development of a chromium-depleted zone adjacent to grain boundaries. This state is referred as "sensitization." Chromium-depleted zones, being anodic with respect to grain interior, are preferentially attacked in the corrosive environment, leading to IGC (Ref. 2). During welding of austenitic stainless steels, particularly of high-carbon content, heat-affected zones (HAZ) of the weldment get sensitized, which adversely affects their resistance against IGC during service in the susceptible environment.

There are several earlier studies involving the use of laser surface melting (LSM) treatment for enhancing corrosion resistance of austenitic stainless steels. However, most of these studies largely involved sensitization repair and dissolution of inclusions for improved IGC and pitting resistance (Refs. 3–10). Laser surface melting of SS dissolves inclusions and regions of segregation to homogenize treated surfaces, thus resulting in marked improvement in pitting resistance (Refs. 5, 8). In sensitized SS, LSM dissolves chromium-rich carbides, thereby releasing chromium back into the matrix, mitigating chromium depletion for enhanced resistance against IGC. Recent research on grain boundaries has shown that sensitization depends strongly on grain boundary character and atomic structure and low-energy grain boundaries such as coincidence site lattice (CSL) boundaries have strong resistance to IGC (Refs. 11–13). Grain boundaries with low-Σ CSL ($\Sigma \leq 29$) are highly resistant against sensitization and IGC. Of late, it has also been demonstrated that the development of extremely randomized grain boundaries result in improved resistance to sensitization, IGC, and IGSCC (Refs. 14, 15). This approach of increasing the fraction of random boundaries to a value above 0.75 has been

KEYWORDS

Laser Welding
Surface Treatment
Stainless Steel
Heat-Affected Zone
Sensitization
Intergranular Corrosion
Grain Boundary

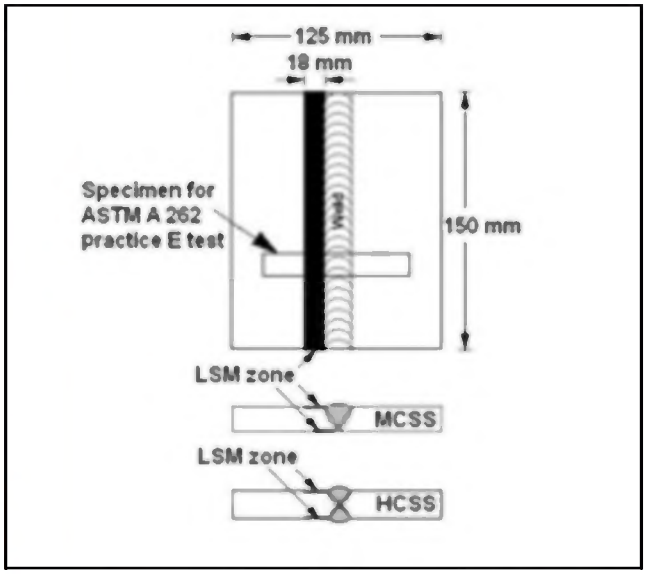

Fig. 1 — Schematic illustration of experimental GTA weldment. Figure also shows specimen for ASTM A 262 Practice E test.

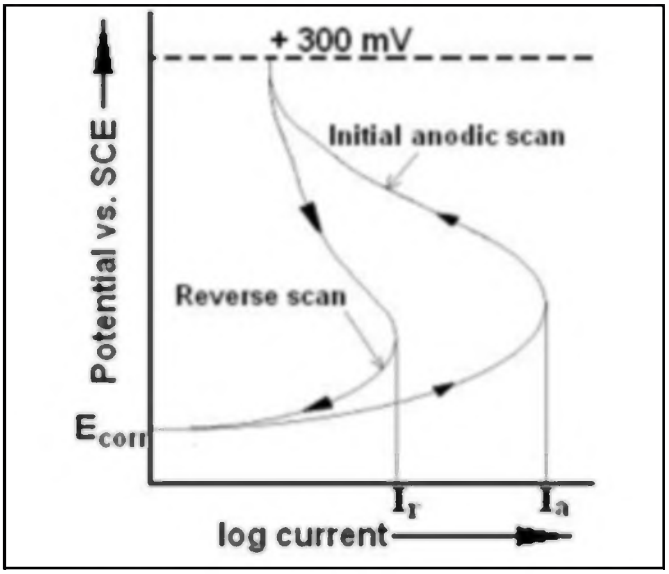

Fig. 2 — Schematic illustration of a typical DL-EPR curve. DOS% = $(I_r/I_a) \times 100$.

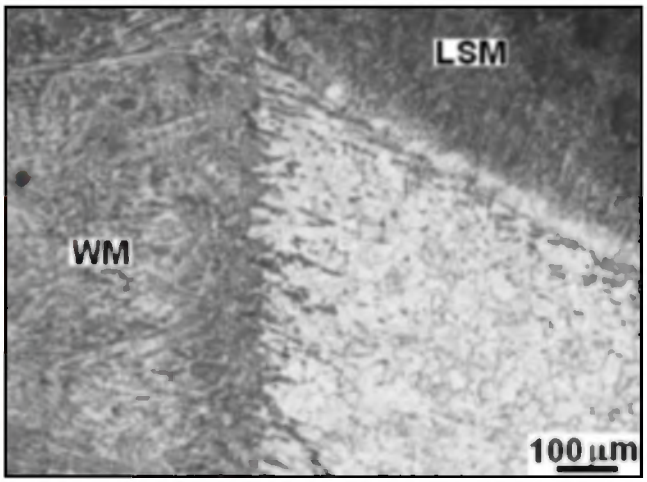

Fig. 3 — Cross section of medium-C SS weldment showing laser surface melted (LSM) zone, adjacent to weld metal (WM).

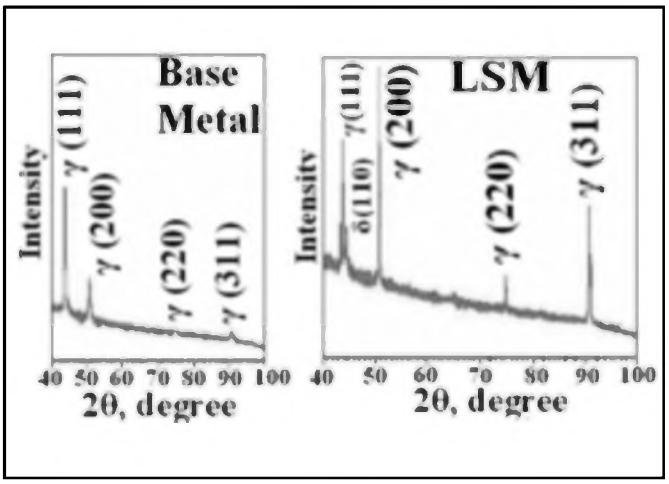

Fig. 4 — XRD patterns of base metal and laser surface melted specimens of medium-C SS.

shown to result in improvement against sensitization. The main reasons given are high diffusion rates of chromium along random grain boundaries and a large number of chromium carbide nuclei formation. The beneficial effect of high fraction of random boundaries was demonstrated in this work through its effect on measurements of degree of sensitization, IGC and IGSCC (Refs. 14, 15). The approach usually adopted for controlling grain boundary character distribution (GBCD) involves thermomechanical treatment for inducing bulk recrystallization. A related study performed in the authors' laboratory has demonstrated that a LSM treatment of 316(N) SS weld metal results in significant increase in its resistance against sensitization during subsequent postweld solution annealing treatment for stress relieving (Ref. 16). A recent work reported by Yang et al. has shown that a combination of LSM and a prolonged heat treatment of 304 SS at 1220 K, resulted in remarkable change in GBCD, thereby resulting in improvement of the resistance against IGC (Ref. 17). The present work was undertaken to develop a prewelding laser surface treatment for the would-be HAZ of Type 304 SS to impart enhanced resistance against sensitization during subsequent gas tungsten arc welding (GTAW). The study demonstrated the validity of the approach on a butt joint weld in sheet steel with a multi-kW CO_2 laser. Application of prewelding treatment with

Table 1 — Chemical Composition (in wt-%) of Stainless Steel Sheets Used for the Study

Base Metal	C	Cr	Ni	Mn	Si	Mo	P	S	Fe
Medium-C SS	0.044	18.16	9.78	1.5	0.48	0.26	0.026	0.015	Bal
High-C SS	0.10	17.8	8.4	1.3	0.51	0.23	—	—	Bal

fiber-delivered laser (Nd:YAG/fiber/diode) would provide additional flexibility to facilitate in-situ pre-welding treatment of the internal surface of tubes/pipes, which often experience IGC during their operation in susceptible environment. Such a technique would be extremely important for austenitic stainless steel weldments operating in hostile environment (e.g., a reprocessing plant), where failures can have serious consequences.

Experimental

This experimental study was performed in two parts. Part 1 of the study was carried out on 6-mm-thick Type 304 SS sheet with a C content of 0.044 wt-%, while the subsequent part of the work was performed on 10-mm-thick Type 304 SS sheet with C content of 0.10 wt-%. The substrates used in Part 1 and Part 2 of the study are referred to as medium-C SS and high-C SS, respectively. Table 1 presents chemical compositions for both base metals (in wt-%), as found out by chemical analysis. Before carrying out laser surface treatment, single-V and double-V grooves (with included angle of 75 deg) were machined in 6- and 10-mm-thick SS sheets, respectively.

The experiments involved surface treatment of would-be heat-affected zones (on both top and bottom surfaces), in one of the two parts to be butt-joint welded, with pulse modulated CO_2 laser beam (LB). Laser surface treatment was carried out with an indigenously developed 4-kW CO_2 laser (Ref. 18). The laser processing setup consisted of the laser system, integrated with a beam delivery system and a computer-controlled 3-axis workstation. The laser beam-emanating out of the laser system, was folded with a 45-deg plane gold-coated copper mirror and subsequently focused with a 127-mm focal length zinc selenide lens, housed in a water-cooled copper nozzle. Laser surface melting treatment involved scanning the surface of the base metal with a defocused LB. The working distance between movable copper nozzle and the specimen (placed below the focal plane) was adjusted to get a beam diameter of 4 mm. During the course of LSM, argon gas flowed through the nozzle to protect the expensive zinc selenide lens from possible spatter at the laser-interaction zone. The laser surface treated part was subsequently gas tungsten arc (GTA) welded to a similar untreated part — Fig. 1. Experimental parameters used for LSM and GTAW are summarized in Table 2. The HAZ developed on the laser-treated and untreated sides of the weld are referred as LSM-HAZ and N-HAZ, respectively. Laser-treated and untreated HAZ specimens were characterized by optical and scanning electron microscopy (SEM), IGC tests as per ASTM A 262 Practices A and E, and double-loop electrochemical potentiokinetic reactivation (DL-EPR) test. In addition, untreated base metal and corresponding laser-treated specimens were also characterized by X-ray diffraction and electron backscattered diffraction (EBSD).

The ASTM A 262 Practice A test is used for rapid screening of the material with respect to sensitization and IGC (Ref. 19). The test involves electrochemical etching of the polished surface of the specimen in 10% oxalic acid solution with a current density of 1 A/cm^2 for 90 s. The test is used for the acceptance of material against IGC. A specimen with "ditch" microstructure in Practice A test may be susceptible to IGC but this susceptibility needs to be tested by another appropriate practice of ASTM A262. On the other hand, ASTM A 262 Practice E test involves exposing the specimens (embedded in copper turnings) to boiling 10%

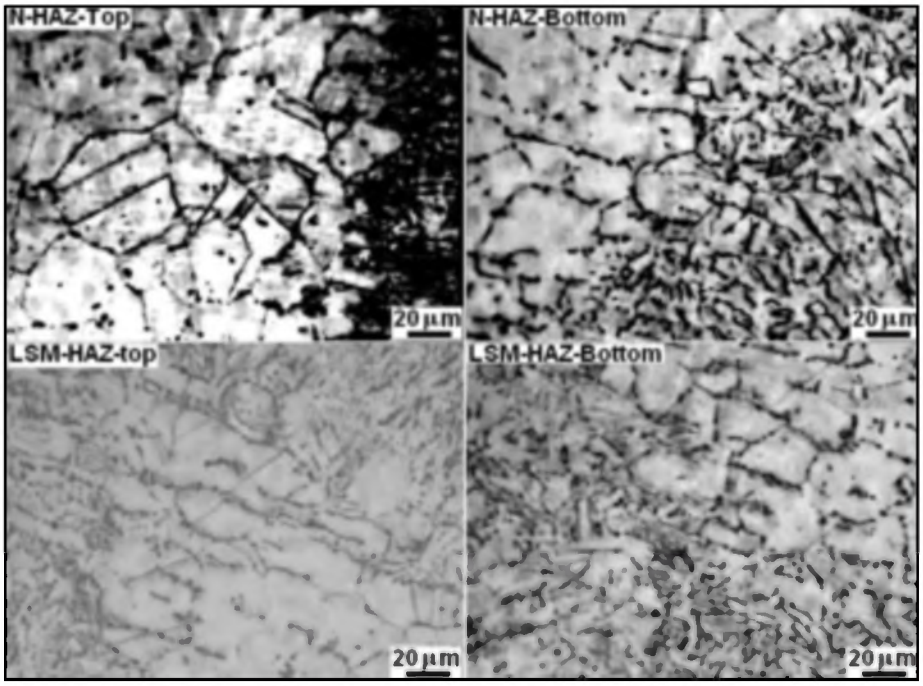

Fig. 5 — Comparison of the microstructures of N-HAZ and LSM-HAZ regions of medium-C SS weldment, as brought out by ASTM A262 Practice A test.

Table 2 — Experimental Parameters Used for LSM and GTAW

Laser Surface Treatment (LSM)							
Peak Power	Base Power	Frequency	Duty Cycle	Beam Diameter	Overlap Between Succesive Tracks		Scan Rate
3.1 kW	0.6kW	100 Hz	50%	4 mm	50%		5 mm/s
Gas Tungsten Arc Welding(GTAW)							
Base Metal	Joint Type	Groove Type	Polarity	Current	Welding Speed	No. of Passes	Welding Wire
Medium-C SS	Butt	Single V	DCEN	70A	2 mm/s	3	1.6 mm diameter
High-C SS	Butt	Double V	DCEN	70A	2 mm/s	5	308L SS

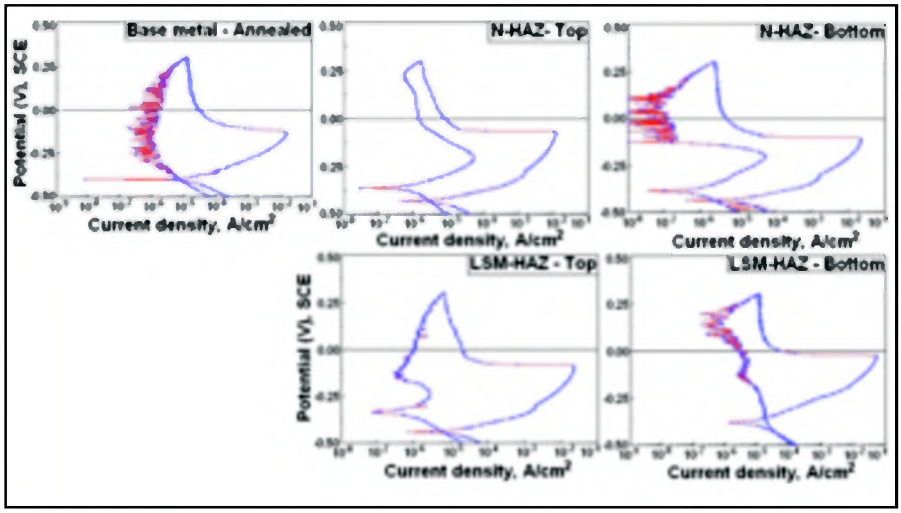

Fig. 6 — Comparison of DL-EPR plots of base metal, LSM-HAZ, and N-HAZ specimens of medium-C SS.

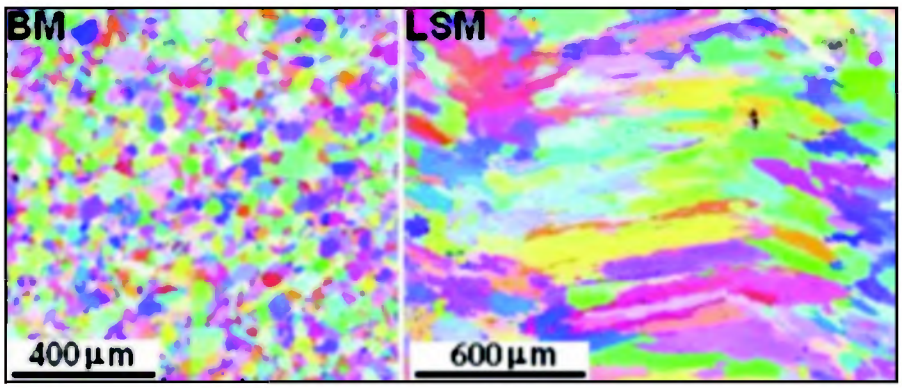

Fig. 7 — Typical result of the investigation performed to measure grain boundary character distributions in base metal (BM) and laser surface melted (LSM) specimens of medium-C SS.

$CuSO_4$-16% H_2SO_4 solution for 24 h. The exposed specimen is subsequently slowly bent with a suitable mandrel in such a way that the zone to be tested (N-HAZ or LSM-HAZ) fell at the center of the bent portion, i.e., subjected to maximum tensile stress (Ref. 19). The specimens in which cracks appeared in the bent portion were categorized as sensitized. Repeating the test in each case checked the reproducibility of the results. The dimensions of the specimens used for Practice E test were 80 mm × 10 mm × thickness, and they were prepared in such a way that each contained weld metal (WM), heat-affected zones (LSM-HAZ and N-HAZ), and base metal, as shown schematically in Fig. 1.

The specimens used for the DL-EPR test were mounted in cold-setting resin in such a way to expose the desired surface. Before specimen mounting, an electrical connection was provided to the specimen by spot welding a metallic wire to its back. Subsequent specimen preparation involved 1) macro-etching the specimens, 2) identification and marking of various zones of the weldment, 3) grinding and diamond polishing up to 0.5 µm finish, and 4) masking with 3M electroplating tape to expose only the HAZ. All the edges of the specimens were masked with lacquer to avoid any crevice attack during the test. The tests were conducted in a de-aerated solution of 0.5 M sulfuric acid and 0.01 M potassium thiocyanate (KSCN). A platinum electrode was used as counter electrode while a saturated calomel electrode (SCE) was used as a reference electrode. The DL-EPR test involved sweeping electrode potential from open circuit potential in the active region to +300 mV (with respect to SCE) in the passive region at the rate of 6 V/h, followed by reverse scan back to the open circuit potential. The basic principle involved in the EPR test involves passivating the specimen's surface, followed by subjecting it to active scan (Ref. 20). In the reverse scan, the resultant current arises mainly from incompletely passivated chromium-depleted zones (Ref. 21). Hence, the charge that passed during reactivation cycle was taken as an index of chromium-depletion. Degree of sensitization (DOS), as determined from the DL-EPR test, is expressed as $DOS\% = (I_r/I_a) \times 100$, where I_r = maximum reactivation current in reverse scan, and I_a = maximum activation current in forward scan, as shown schematically in Fig. 2 (Refs. 22, 23). For characterizing each zone of the weldment, one specimen was used for the DL-EPR test. Various specimens, used for the DL-EPR test, were extracted from the central region of the welded plate.

Electron backscattered diffraction (EBSD) (Refs. 14, 24, 25) was used to characterize the respective microtextures. A Quanta 200HV SEM (scanning electron microscope) with a TSL-EDX OIM (orientation imaging microscopy) or EBSD system was used. The EBSD samples were electropolished using standard technique (Ref. 14). Beam and video conditions were kept identical between the scans. For phase identification, between FCC austenite and BCC ferrite, a minimum of 5 Kikuchi bands was used. Grain boundary nature (Ref. 26) was characterized by coincident site lattice (CSL) notation. It needs to be noted that the CSL nature can affect dramatically the grain boundary energy (Ref. 26), and in turn, may determine the sensitization response (Ref. 14). CSL boundaries were identified from OIM data using Brandon's criterion (Ref. 27):

$$\Delta\theta = 15°\Sigma^{-1/2}$$

where $\Delta\theta$ is the angular deviation from the exact CSL and Σ is the type of CSL boundary (Refs. 28–30).

The grain boundary nature (Refs.

Table 3 — Results of DL-EPR Tests

Specimen		%Degree of Sensitization (DOS)	
		Top Surface	Bottom Surface
Medium-C SS	Base Metal	No reactivation peak	
	N-HAZ	0.45	0.26
	LSM-HAZ	0.0123[a]	0.0109[a]
High-C SS	Base Metal	0.0003	
	N-HAZ	12.38	42
	LSM-HAZ	0.031[a]	0.029[a]

(a) After removing oxide layer and corrugations present on laser-melted surface.

28–30), between different samples, can be collated in terms of possible differences in energy (Refs. 30, 14). The low-angle and the low-Σ boundaries are expected to have lower energies than the so-called random boundaries (Refs. 28–30, 14). This energy, however, depends on the exact CSL nature and also on the grain size. In an earlier study (Ref. 14), it was proposed to bring in a single parameter defining the grain boundary nature. This parameter, termed generically as effective grain boundary energy (EGBE), considered fractions of different types of CSL (f_i) with stipulated (Ref. 31) differences in CSL energy (γ_i). EGBE = $((\Sigma\gamma_i f_i)4/d))/\gamma_{max}$) (Ref. 14), where γ_i for respective CSL was calculated using the general formula $\gamma_{CSL} = (1-1/\sqrt{\Sigma})\,\gamma_{max}$ (Ref. 31). The formalism, though used effectively in bringing out effects of grain boundary nature on DOS (Ref. 14), has two problems. Firstly, it does not consider possible differences in tilt-twist nature of the boundaries. Secondly, it does not consider the deviation from exact CSL nature. Two-dimensional EBSD measurements are incapable of resolving the first issue. The second issue can, however, be estimated and incorporated in an EGBE formula. The modified EGBE formulation, as used in the present study, is indeed an improvement over the earlier formalism and has been used for studies on sensitization (Ref. 32) and also to define developments in grain boundary nature with thermomechanical processing (Ref. 33).

The existing CSL model (Refs. 28–30) for grain boundaries accounts for two-dimensional misfits, but this may not be adequate in giving a three-dimensional misfit or an effective index of energy (Refs. 34, 35). For example, Σ3 twin boundaries have completely different energies based on their tilt or twist nature, though the CSL notation in both cases remains the same (Refs. 28, 30). The boundary nature can also be affected by the solute presence (Refs. 28, 30). In spite of such limitations, CSL theory, in general, and EGBE, in particular, have been quite effective in defining the grain boundary nature and relating the same with sensitization behavior in austenitic stainless steel. The present study also shows a relationship between DOS and EGBE before and after laser treatment.

Results

Part 1: Conducted on Medium Carbon Type 304 Stainless Steel

Optical Microscopy

Optical microscopic examination of the transverse cross section of the weldment revealed the presence of overlapping laser surface melted tracks of about 600 μm depth on one side of the GTA weld. Laser surface melted zones exhibited typical cellular/dendritic microstructure. Figure 3 presents an optical photomicrograph of the transverse cross section of the weldment showing laser surface melted zone adjacent to weld metal (WM).

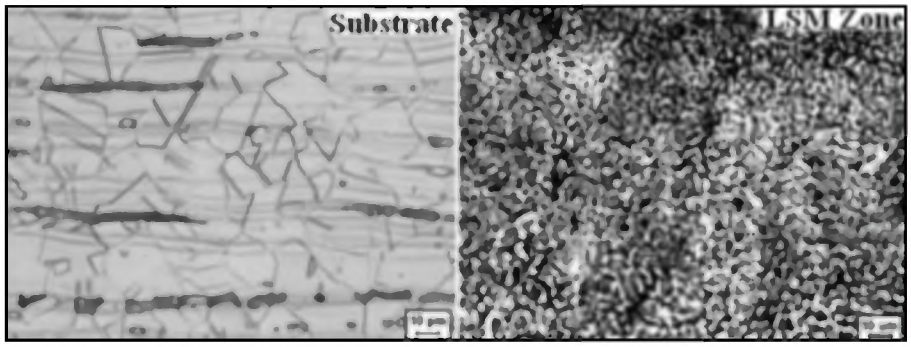

Fig. 8 — Microstructures of the substrate and laser-melted zone (LSM) of high-C SS, as brought out by ASTM A 262 Pr. A test.

X-Ray Diffraction (XRD)

X-ray diffraction, performed on laser surface melted and untreated base metal specimens, demonstrated that, in contrast to, single-phase austenite microstructure of untreated base metal, laser melted surface was associated with duplex microstructure of austenite and δ-ferrite, as shown in Fig. 4. The amount of δ-ferrite present on laser-melted surface was estimated as 4.3%.

IGC Test: ASTM A262 Practice A

Heat-affected zones, developed on the two sides of WM (i.e., LSM-HAZ and N-HAZ), exhibited dual microstructures with discontinuous carbide precipitation along the grain boundaries. However, compared to the N-HAZ specimen, the width of the chromium-depleted zone in LSM-HAZ specimens was reduced and carbide precipitation became more discontinuous. Figure 5 compares microstructures of LSM-HAZ and N-HAZ near top and bottom surfaces of the weldment.

Double-Loop Electrochemical Potentiokinetic Reactivation (DL-EPR) Test

In order to compare DOS, induced by GTAW in LSM-HAZ and N-HAZ of gas tungsten arc weldment, DL-EPR test (Refs. 36–38) was performed on the top and bottom surfaces of the specimens extracted from the concerned regions of medium-C SS weldment. The test results demonstrated a high value of DOS% (1.12) of top LSM-HAZ surface. It should be noted that the examined surface at this stage carried surface irregularities and oxide layers, introduced by LSM and subsequent welding operation. The value of DOS% rapidly reduced as the specimen was sequentially polished off. At a depth of about 100–150 μm from the top of the treated surface, DOS% dropped to very low value of 0.0123, confirming the highly passivating nature of LSM-HAZ. The exposed surface at this stage was free of surface irregularities and all traces of oxide layer. On the other hand, all four N-HAZ specimens exhibited largely similar DOS% values viz. 0.45 and 0.26 for top and bottom surfaces, respectively. The results of DL-EPR tests are summarized in Table 3 and Fig. 6. It should be mentioned that the DOS% reported here is the average of 2 tests and the values vary within ± 0.01%.

Table 4 — Results of ASTM A262 Practice E Tests

Specimen	Zone under Testing	Surface under Testing	Result
Medium-C SS	"N-HAZ"	Top Surface	Uncracked
		Bottom Surface	Uncracked
	"LSM-HAZ"	Top Surface	Uncracked
		Bottom Surface	Uncracked
High-C SS	"N-HAZ"	Top Surface	Specimen broke into two parts
		Bottom Surface	Specimen broke into two parts
	"LSM-HAZ"	Top Surface	Uncracked
		Bottom Surface	Uncracked

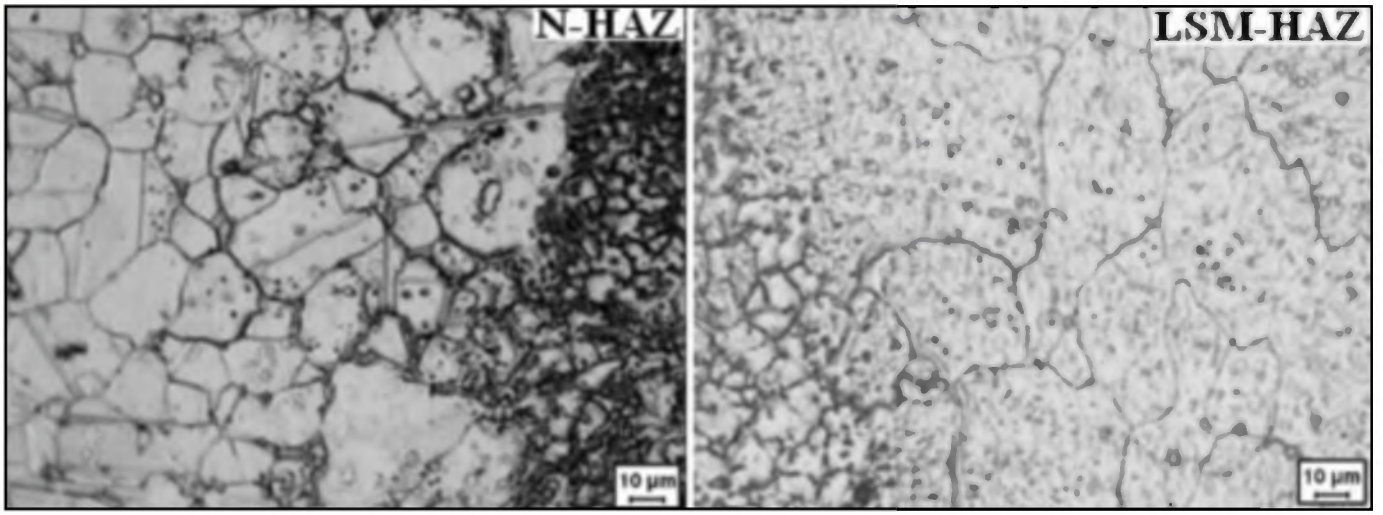

Fig. 9 — Microstructures of untreated HAZ (N-HAZ) and laser treated HAZ (LSM-HAZ) of high-C SS, as brought out by ASTM A 262 Pr. A test.

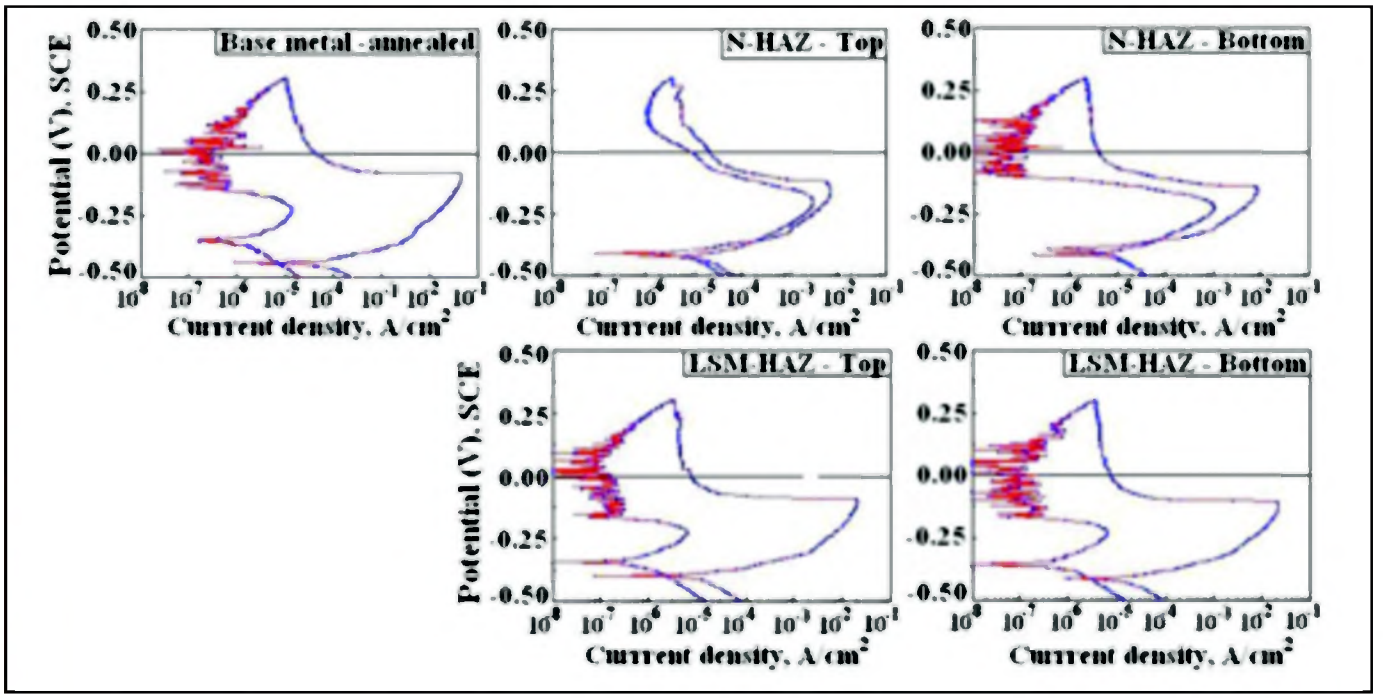

Fig.10 — Comparison of DL-EPR plots of base metal, N-HAZ, and LSM-HAZ specimens of high-C SS.

The reproducibility was achieved by keeping the time between polishing and electrochemical testing exactly the same for both specimens.

IGC Test: ASTM A262 Practice E

ASTM A262 Practice E test was conducted on four different specimens (two each from LSM-HAZ and N-HAZ) taken out of the weldment. Out of the two specimens of each kind, one was bent with top surface in tension (i.e., on the convex side) while the other specimen was bent with bottom surface in tension. All four tested specimens passed the test, indicating that heat-affected zones, developed on both the sides of WM remained unsensitized, and hence, not susceptible to IGC. Test results are summarized in Table 4.

Electron Backscattered Diffraction

Electron backscattered diffraction (EBSD) analysis revealed that the fraction of $\Sigma 1$ boundaries (with angle of misorientation $\Delta\theta$ = 1–15 deg) in the base metal was 0.04 and it increased to 0.13–0.19 after LSM. Figure 7 presents the typical result of the investigation carried out to measure grain boundary character distribution in base metal and laser surface melted specimen.

Part 2: Conducted on High-Carbon Type 304 Stainless Steel Sheet

IGC Test: ASTM A262 Practice A

The base metal, in solution annealed condition, exhibited step microstructure with banding and isolated carbide precipitation at grain boundaries, as shown in Fig. 8. The base metal was associated with heterogeneity in microstructure (in terms

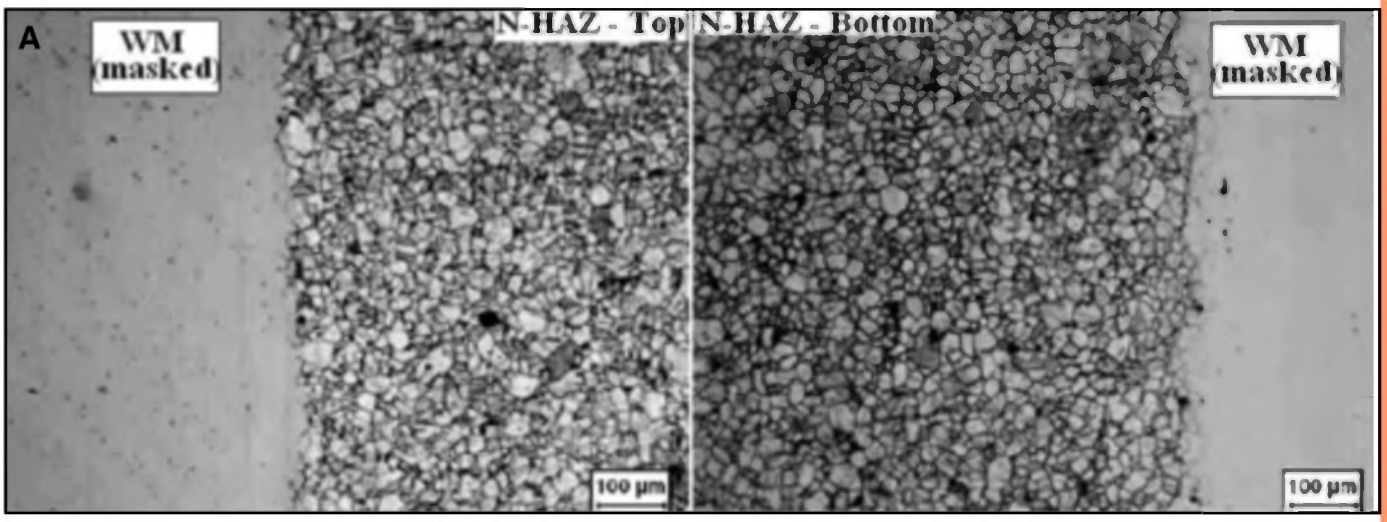

of carbide precipitation) across its thickness. Metallographic examination of laser treated specimens exhibited a surface melted layer with thickness in the range of 270–500 µm. Laser surface melted zone was associated with typical cast microstructure, as shown in Fig. 8. On the other hand, the N-HAZ specimen exhibited ditch microstructure, while the LSM-HAZ specimen was associated with lightly etched grain boundaries, indicating relatively lower value of chromium-depletion at the grain boundaries than that in N-HAZ specimen. Figure 9 presents microstructures of N-HAZ and LSM-HAZ specimens, as revealed by ASTM A 262 Practice A test.

Double-Loop Electrochemical Potentiokinetic Reactivation Test

Double-loop electrochemical potentiokinetic reactivation (DL-EPR) tests were performed on top and bottom surfaces of N-HAZ and LSM-HAZ specimens of high-C SS. On the basis of the results of first part of the study, treated surfaces of LSM-HAZ specimens were polished to remove surface irregularities and oxide layers before conducting DL-EPR tests. The results of the tests demonstrated that GTAW brought about very large increase in DOS% in the untreated HAZ (N-HAZ). Base metal specimen in the solution annealed condition exhibited a DOS% of 0.0003, whereas the DOS% of N-HAZ specimens from top and bottom surfaces was 12.38 and 42, respectively. In sharp contrast, LSM-HAZ specimens, exposed to similar thermal history, recorded significantly lower DOS% than their N-HAZ counterparts. The DOS of LSM-HAZ specimens taken from top and bottom surfaces were 0.031% and 0.029%, respectively. Results of DL-EPR tests are summarized in Fig. 10 and Table 3. It is believed that the difference in DOS% of top and bottom surfaces of the N-HAZ specimens is caused by microstructural inhomogeneity present in the base material. Optical microscopic examination of DL-EPR tested N-HAZ specimens revealed chromium-depleted zones along grain boundaries — Fig. 11A. On the other hand, LSM-HAZ specimens exhibited lightly etched grain boundaries — Fig. 11B, indicating significantly reduced chromium-depletion at the grain boundaries than that observed in N-HAZ specimens.

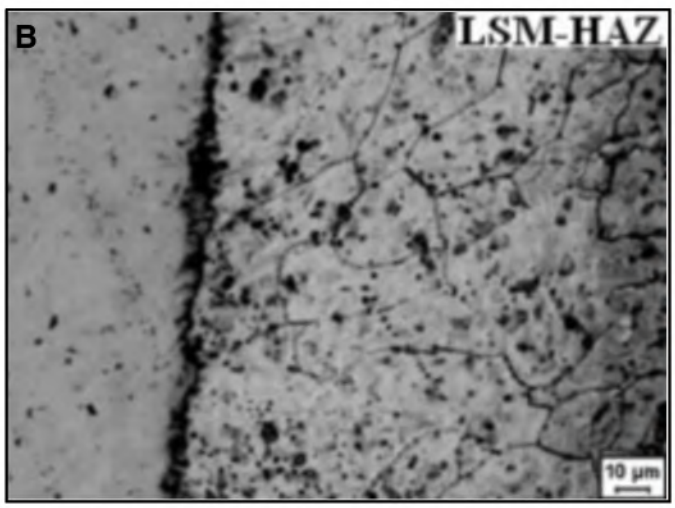

Fig. 11 — A — Magnified views of DL-EPR tested untreated HAZ (N-HAZ) specimens of high-C SS; B — magnified view of DL-EPR tested laser treated HAZ (LSM-HAZ) specimens of high-C SS.

IGC Test: ASTM A262 Practice E

ASTM A262 Practice E test was conducted on four numbers of specimens (two each for N-HAZ and LSM-HAZ), taken out from high-C SS weldment — Fig. 1. The two numbers of N-HAZ specimens broke into two pieces. In sharp contrast, both LSM-HAZ specimens remained uncracked, as shown in Fig. 12. Table 4 summarizes the results of ASTM A262 practice E test.

Electron Backscattered Diffraction

Electron backscattered diffraction analysis of untreated base metal and laser surface melted specimens of high-C SS revealed that LSM brought about an increase in the percentage fraction of Σ1 boundaries ($\Delta\theta$ = 1–15 deg) from 0.536 (in the base metal) to 0.759 (on laser melted surface). Figure 13A presents typical results of the experiments carried out to measure GBCD in base metal and laser surface melted specimen. Further analysis of EBSD data, as presented in Fig. 13B, revealed that the bulk of Σ1 boundaries in laser-melted specimen belongs to subgrain boundaries, introduced by melting and resolidification. On the contrary, Σ1 grain boundaries constitute a major part of total Σ1 boundaries in the base metal. In addition, LSM also brought about considerable reduction in the percentage fraction of Σ3 coherent twin boundaries — from 0.1905 (in the base metal) to 0.03 (on laser-melted surface). Microstructural modification, induced by LSM, resulted in significant reduction in effective grain boundary energy (EGBE) from 1.12 (in the base metal) to 0.459 (on the laser melted surface).

Another important output of EBSD analysis is that laser-melted surface carried very little amount of delta-ferrite in a largely austenitic matrix. The fraction of delta ferrite in the base metal and on laser-melted surface was estimated as 0.7% and 0.3%, respectively. Figure 13C presents austenite-ferrite map of the microstructures of base

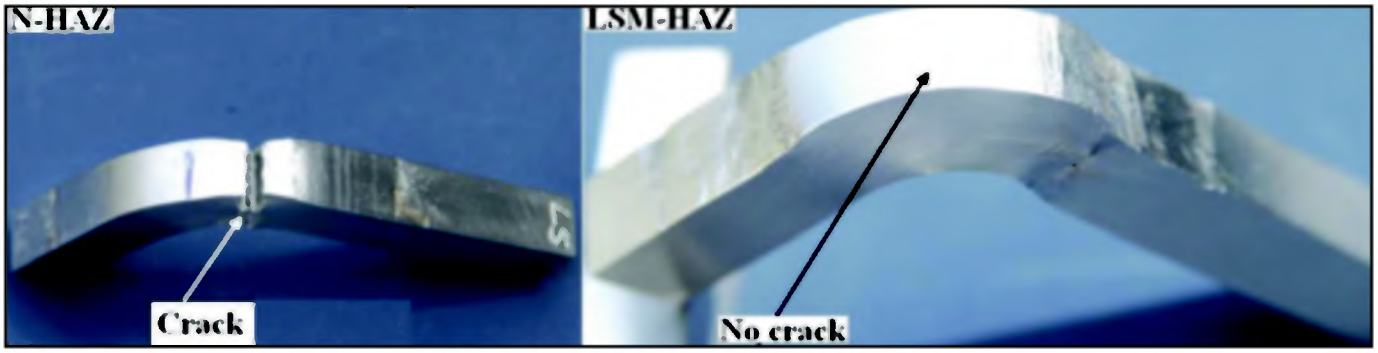

Fig. 12 — Magnified views of untreated HAZ (N-HAZ) and laser treated HAZ (LSM-HAZ) specimens of high-C SS after undergoing IGC test as per ASTM A 262 Practice E.

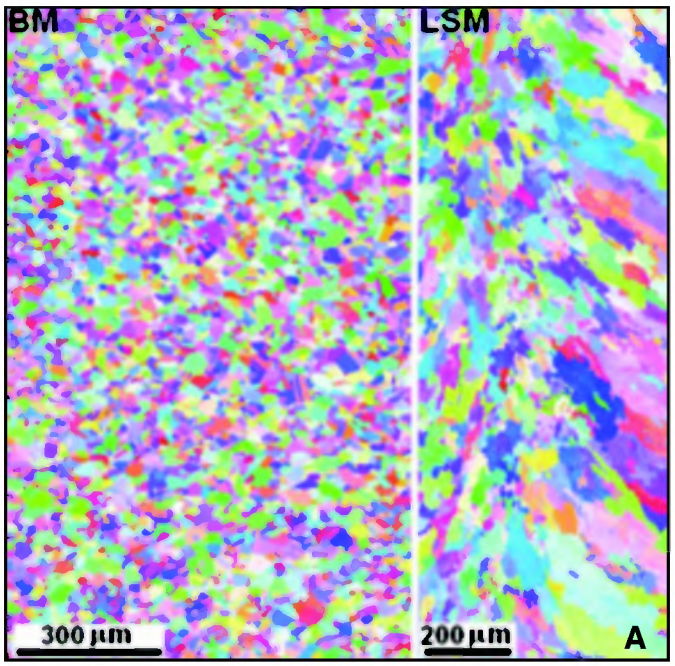

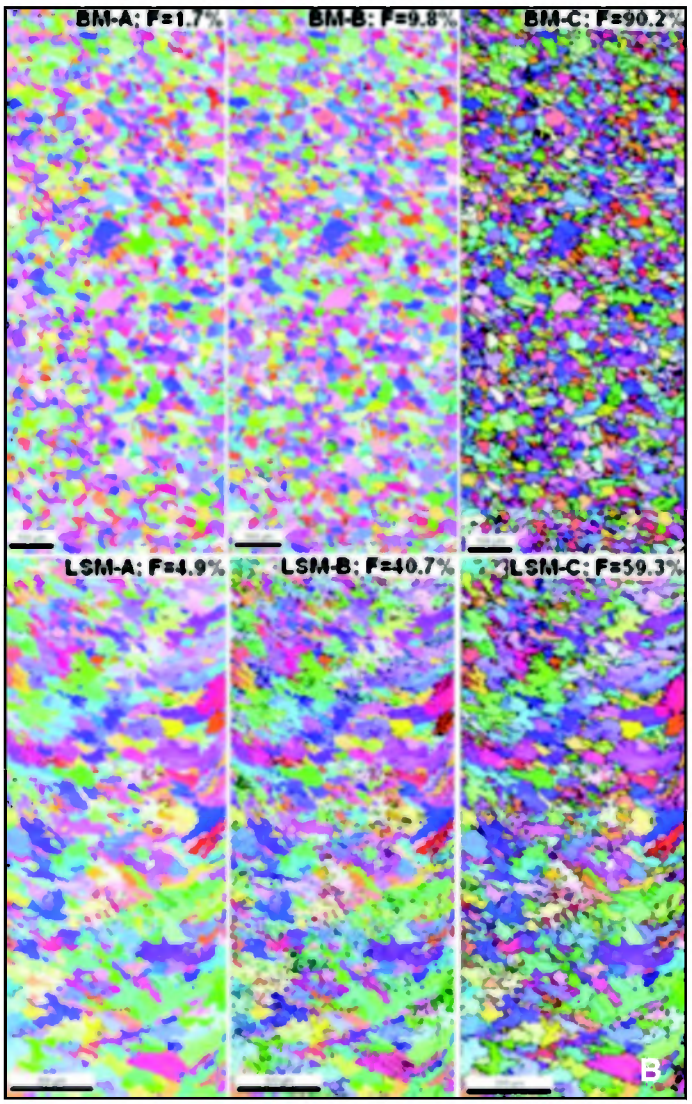

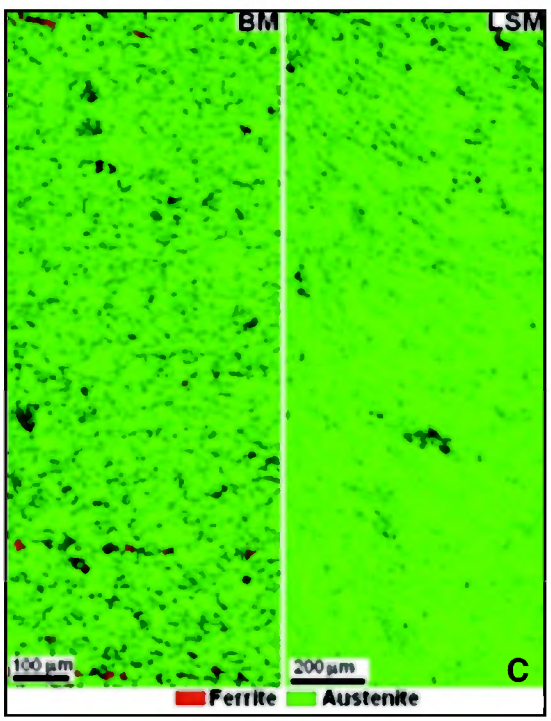

Fig. 13 — A — Typical result of the investigation performed to measure grain boundary character distributions in base metal (BM) and laser surface melted (LSM) specimens of high-C SS; B — typical distributions of (A) Σ1 boundaries (Δθ =1–15 deg) between identifiable grains, (B) all Σ1 boundaries (Δθ = 1–15 deg), and (C) high-angle grain boundaries (Δθ =15–180 deg) in base metal (BM) and laser surface melted (LSM) specimens. Concerned boundaries are marked in black whereas associated percentage fractions (F) are indicated on respective images; C — EBSD-generated austenite/ferrite phase maps of the microstructure of base metal (BM) and laser surface melted (LSM) specimens of high-C SS.

metal and laser-melted surface.

Synthesis of Results and Discussion

The results of first part of the study, conducted on 6-mm-thick Type 304 SS sheet with carbon content of 0.044 wt-%, demonstrated that microstructural modification induced by GTAW resulted in the development of a moderate degree of sensitization (0.26% and 0.45% for top and bottom surfaces, respectively) on the surface of untreated HAZ. A prewelding surface treatment of the would be HAZ with pulse-modulated LB, brought about a reduction in DOS of the resultant HAZ. Because of relatively lower value of C content and moderate heat input associated with 3-pass GTAW of 6-mm-thick medium-C SS sheet, the DOS induced in the HAZ was not very significant and as a result, degree of LSM-induced improvement in the DOS% of HAZ was not very prominent. This fact is reflected in both untreated and laser-treated HAZ specimens passing ASTM A 262 Practice E test.

The results of the first part of the study, although indicated an increase in materials resistance against sensitization, did not establish strong effectiveness of the technique in suppressing sensitization due to moderate level of C content and heat input associated with GTAW of 6-mm-thick SS sheet. Hence, in Part 2 of the study, LSM treatment approach was evaluated on 10-mm-thick Type 304 SS plate of high-C content (0.1 wt-%), where welding-induced microstructural damage in the HAZ was expected to be significantly extensive. Results of second part of the study exhibited that 5-pass GTAW brought about extensive sensitization in the untreated HAZ of high-C SS. As a result of GTAW, the DOS% of material rose from 0.0003 (in the base metal in solution annealed condition) to extremely high values of 12.38% and 42% on the top and bottom surfaces of untreated HAZ, respectively. In sharp contrast, DOS of laser surface treated HAZ specimens (LSM-HAZ) remained at very low level (0.03), even after experiencing similar thermal exposure. Extremely large reduction in DOS% brought about by prewelding LSM treatment, even under extremely adverse conditions (combination of high-C concentration and large heat input), underlines strong effectiveness of LSM treatment in suppressing HAZ sensitization during subsequent GTAW. The large difference in the DOS% between N-HAZ and LSM-HAZ specimens is translated into large difference in their susceptibilities against IGC. This fact is reflected in laser-treated HAZ specimen successfully passing IGC test as per ASTM A 262 Practice E, in sharp contrast to untreated HAZ specimens, which broke into two pieces. It should be noted here that in order to realize maximum beneficial effect, surface undulations introduced by LSM treatment should be removed before the parts are welded.

The EBSD analysis, performed on both medium-C and high-C SS specimens, demonstrated that LSM brought about significant increase in the fraction of $\Sigma 1$ boundaries. In the case of high-C SS specimens, the increase in the fraction of $\Sigma 1$ boundaries is reflected in about 2.5 times drop in effective grain boundary energy. $\Sigma 1$ boundaries, with small angle of misorientation ($\Delta\theta$ = 1–15 deg), are characterized by low energy, slow transport properties (e.g., grain boundary chemical and thermal diffusion, grain boundary migration and sliding) as compared to high angle grain boundaries. These boundaries, because of their low energy, are more resistant to nucleation of chromium carbides. Hence, such boundaries are more resistant to sensitization (Refs. 14, 23). The increased fraction of low-angle boundaries on the laser melted surface is largely attributed to large increase in subgrain boundaries associated with fine subgrain features (like dendrites, cells, etc.), arising as a result of melting and resolidification. It is believed that these subgrain boundaries introduce frequent disruptions in random grain boundary network, thereby resulting in enhanced resistance against IGC. It should be noted that unlike duplex (austenite + ferrite) microstructure of laser-melted surface of medium-C SS, the same treatment generated a largely austenitic microstructure in high-C SS. In spite of this difference in ferrite content on the laser-treated surface, both kinds of laser-melted specimens exhibited enhanced resistance against sensitization and IGC. Hence, the large reduction in the DOS and susceptibility to IGC, brought about LSM, is primarily contributed by significant increase in the fraction of $\Sigma 1$ subgrain boundaries associated with resolidified microstructure on the surface.

Conclusions

The present study demonstrated that laser surface melting treatment of the would be heat-affected zones of Type 304 SS components results in a surface microstructure with significantly enhanced resistance against sensitization during subsequent GTAW operation. The reason for enhanced resistance of laser-melted surface against sensitization and IGC is attributed to a significant increase in the fraction of $\Sigma 1$ boundaries (mostly subgrain boundaries), introduced by melting and resolidification. Frequent disruptions in the random grain boundary network by intersecting subgrain boundaries is believed to be the cause for its enhanced resistance against sensitization and IGC. In light of the results of the study, a new noncontact prewelding laser surface treatment approach is proposed for GTA weldments of austenitic stainless steel to effectively enhance their resistance against HAZ sensitization and IGC. The proposed technique has a great potential in enhancing the life of austenitic stainless steel welded components operating in corrosive environments, especially prevalent in the process industry.

Acknowledgments

The authors are extremely thankful to R. K. Soni and Harish Kumar for their contributions during various stages of the present investigation. Technical assistance of J. B. Rathi, A. R. Adbol, B. S. Rawat, Ram Nihal Ram, and A. P. Singh is thankfully acknowledged.

References

1. Andresen, P., Morra, M., and Catlin, W. 2004. Effects of yield strength, corrosion potential, composition, and stress intensity factor on SCC of stainless steels. *Proc. CORROSION-2004*, paper no. 04678, NACE International.

2. Stainless Steel. 1993. Edited by P. Lacombe, B., Baroux, and G. Beranger. *Les Editions de Physique Le Ulis*, pp. 406–415.

3. Conde, A., Colaço, R., Vilar, R., and Damborenea, J. de. 2000. Corrosion behavior of steels after laser surface melting. *Material & Design* 21(5): 441–445.

4. Mudali, U. K., Dayal, R. K., and Goswami, G. L. 1998. Laser surface melting for improving intergranular corrosion resistance of cold-worked and sensitised Type 316 stainless steel. *Anti-Corros. Methods Mater.* 45(3): 181–188.

5. Carboni, C., Peyre, P., Beranger, G., and Lemaitre, C. 2002. Influence of high power diode laser surface melting on the pitting corrosion resistance of Type 316L stainless steel. *J. Mat. Sci.* 37(17): 3715–3723.

6. Jeng, J. Y., Quayle, B. E., Modern, P. J., Steen, W. M., and Bastow, B. D. 1993. Laser surface treatments to improve the intergranular corrosion resistance of 18/13/Nb and 304L in nitric acid. *Corr. Sci.* 35(5–8): 1289–1296.

7. Song, Q., and Shen, L. 1997. Microstructural features of laser surface melting 1Cr17Ni2 stainless steel. *Scripta Materialia* 36(5): 531–534.

8. Chong, P. H., Liu, Z., Wang, X. Y., and Skeldon, P. 2004. Pitting corrosion behavior of large area laser surface treated 304L stainless steel. *Thin Solid Films* 453–454: 388–393.

9. Chong, P. H., Liu, Z., Skeldon, P., and Crouse, P. 2005. Characterization and corrosion performance of laser-melted 3Cr12 steel. *Appl. Surf. Sci.* 247(1–4): 362–368.

10. Chandra, K., Kain V., and Ganesh, P. 2008. Controlling end-grain corrosion of austenitic stainless steels. *J. Mater. Eng. Perform.* 17(1): 115–122.

11. Palumbo, G., and Aust, K. T. 1990. Structure dependence of intergranular corrosion in high-purity nickel. *Acta Metallurgica et Materialia* 38(11): 2343–2352.

12. Lin, P., Palumbo, G., Erb, U., and Aust,

K. T. 1995. Influence of grain boundary character distribution on sensitization and intergranular corrosion of Alloy 600. *Scripta Metallurgica et Materialia* 33(9): 1387–1392.

13. Kokawa, H., Shimada, M., and Sato, M. 2000. Grain-boundary structure and precipitation in sensitized austenitic stainless steel. *Journal of Materials* 52(7): 34–37.

14. Wasnik, D. N., Kain, V., Samajdar, I., Verlinden, B., and De, P. K. 2002. Resistance to sensitization and intergranular corrosion through extreme randomization of grain boundaries. *Acta Materialia* 50(18): 4587–4601.

15. Wasnik, D. N., Kain, V., Samajdar, I., Verlinden, B., and De, P. K. 2003. Controlling grain boundary energy to make austenitic stainless steels resistant to intergranular stress corrosion cracking. *Journal of Materials Engineering and Performance* 12(4): 402–407.

16. Parvathavarthini, N., Dayal, R. K., Kaul, R., Ganesh, P., Khare, J., Nath, A. K., Mishra, S. K., and Samajdar, I. 2008. Novel laser surface treatment approach to suppress sensitization in modified Type 316(N) stainless steel weld metal. *Science and Technology of Welding and Joining* 13(4): 335–343.

17. Yang, S., Wang, Z. J., Kokawa, H., and Sato, Y. S. 2007. Grain boundary engineering of 304 stainless steel by laser surface melting and annealing. *J. Mat. Sci.* 42(3): 847–853.

18. Khare, J., Sridhar, R., Paul, C. P., Reghu, T., and Nath, A. K. 2003. Optical characteristics and power scaling of a transverse flow transversely excited CW CO_2 laser. *Pramana* 60(1): 99–107.

19. ASTM A262-2004, Annual book of ASTM standards 1990, Section 3 Metals test methods and analytical procedures: Vol. 03.02 *Wear and Erosion, Metal Corrosion*, Philadelphia, Pa.: ASTM, 1992.

20. Cihal, V., Štefec, R., Shoji, T., Watanabe, Y., and Kain, V. 2004. Electrochemical potentiodynamic reactivation: development and applications of the EPR test, *Key Engineering Materials*. 261–263: 855–864.

21. Dayal, R. K., Parvathavarthini, N., and Raj, B. 2005. Influence of metallurgical variables on sensitization kinetics in austenitic stainless steels. *Int. Mat. Rev.* 50(3): 129–155.

22. Revised committee draft ISO/CD-12372 for a proposed standard on Method for EPR Test. 1998. ISO-Technical Committee 156, 7th revised version.

23. Clarke, W. L., Cowan, R. L., and Walker, W. L. 1978. *Comparative Methods for Measuring Degree of Sensitization in Stainless Steel*. ASTM Special Technical Publication STP 656, West Conshohocken, Pa., ASTM International, p. 99.

24. Introduction to Orientation Imaging Microscopy, *www.stanford.edu/group/snl/SEM/OIMIntro.htm*., visited on Dec. 05, 2008.

25. Adams, B. L., Wright, S. I., and Kunz, K. 1993. Orientation imaging: the emergence of a new microscopy. *Metall. Mater. Trans. A* 24(4): 819–831.

26. Murr, L. E. 1975. *Interfacial Phenomena in Metal and Alloys*, Reading, Mass., Addison Wesley Publishing Co.

27. Brandon, D. G. 1966. *Acta Metall*. 14: 1479.

28. Randle, V. 1996. *The Role of Coincident Site Lattice in Grain Boundary Engineering*, The Institute of Materials, UK.

29. Smith, D. A., and Pond, R. C. 1976. *Int. Metals Rev*. 21: 61.

30. Verlinden, B., Driver, J., Samajdar, I., and Doherty, R. D. 2007. *Thermo-Mechanical Processing of Metallic Materials*, ISBN–978-0-08-044497-0, Pergamon Materials Series. Series ed. R.W. Cahn, Elsevier, Amsterdam.

31. Aleshin, A. N., Aristov. V. Yu, Bokshtein, B. S., and Shvindlerman, L. S. 1978. Kinetic properties of <111> tilt boundaries in aluminum. *Physica Status Solidi* (*A*) 45(1): 359–366.

32. Parvathavarthini, N., Dayal, R. K., Raj, B., Mulki, S., Samajdar, I., and Mani, K. V. 2009. Sensitization control in AISI 316L(N) austenitic stainless steel: defining the role of grain boundary nature. *Corr. Sci.* (in press).

33. Karthikeyan, T., Paul, V. T., Mishra S., Saroja, S., Vijayalakshmi, M., and Samajdar, M. 2009. Effect of thermomechanical treatment on the grain boundary character distribution in a 9Cr-1Mo ferritic steel, *Met. Trans A* (in press).

34. Manikrishna, K. V., Sain, A., Samajdar, I., Dey, G. K., Srivastava, D., Neogi, S., Tiwari, R., and Banerjee, S. 2006. Resistance to hydride formation in zirconium: an emerging possibility. *Acta Mater.* 54: 2665–2675.

35. Hiwarkar, V. D., Sahoo, S. K., Manikrishna, K. V., Samajdar, I., Dey, G. K., Srivastav, D., Tewari, R., Banarjee, S., and Doherty, R. D. 2009. Coarsening of second phase in a two-phase Zr-2.5 Nb: on the role of phase boundaries. To be submitted to *Acta Mater.*

36. Kain, V., Prasad, R. C., and De, P. K. 2002. Testing sensitization and predicting susceptibility to intergranular corrosion and intergranular stress corrosion cracking in austenitic stainless steels. *Corrosion* 58(1): 15–37.

37. Cihal, V., Shoji, T., Kain, V., Watanabe, Y., and Štefec, R. 2004. *EPR — A Comprehensive Review*, Sendai, Japan, FPRI Publication.

38. Majidi, A. P., and Streicher, M. A. 1984. The double loop reactivation method for detecting sensitization in AISI 304 stainless steel. *Corrosion* 40(11): 584–593.